

To Verify Frame-Dragging: The Asymmetric Response of LARES 2 and LAGEOS to Tidal Perturbations

Xizhi Hu^{1,4}, Xiaodong Chen^{2*,4}, Jianqiao Xu^{1,4}, Ignazio Ciufolini^{3,5}, Wei-Tou Ni^{6,7}, Antonio Paolozzi⁵

¹ State Key Laboratory of Precision Geodesy, Innovation Academy for Precision Measurement Science and Technology, CAS, Wuhan 430077, China

² Wuhan National Observation and Research Station for Geodesy, Innovation Academy for Precision Measurement Science and Technology, CAS, Wuhan 430077, China

³ Wuhan Institute of Physics and Mathematics, Innovation Academy for Precision Measurement Science and Technology, Chinese Academy of Sciences, Wuhan 430071, China

⁴ College of Earth and Planetary Sciences, University of Chinese Academy of Sciences, Beijing 100049, China

⁵ Scuola di Ingegneria Aerospaziale, Sapienza Università di Roma, Rome 00138, Italy

⁶ Lanzhou Center for Theoretical Physics and Key Laboratory of Theoretical Physics of Gansu Province, Lanzhou University, Lanzhou 730000, China

⁷ International Center for Theoretical Physics Asia-Pacific, University of Chinese Academy of Sciences, Beijing 100190, China

* Corresponding author (email: chenxd@apm.ac.cn)

Abstract Laser-ranged satellites have demonstrated exceptional effectiveness in high-precision verification of General Relativity but also in the accurate inversion of geophysical parameters such as Earth tidal parameters. Due to the extremely weak frame-dragging signal, after utilizing the orbital symmetry of LARES 2 and LAGEOS satellites to cancel most of the nodal precession caused by Earth's oblateness, precise modeling of incompletely symmetric Earth tidal perturbation patterns becomes the core prerequisite for effectively extracting this signal. This study, based on Kaula's perturbation theory and Lagrange equations, investigates the perturbations of LARES 2 and LAGEOS satellite orbital nodes and inclinations caused by Earth tides. From the tidal perturbations computed from 402 earth tide constituents, 83 tidal perturbations with significant amplitudes were selected by threshold based on the RMS of overlap orbit differences of the two satellites, the asymmetric characteristics of tidal perturbations between the two satellites were quantitatively analyzed. The traditional amplitude threshold method for individual tidal perturbations is limited, as the coherent superposition of minor tidal constituents and frequency-orbit resonance lead to the total effect exceeding the threshold. These results provide important support for high-precision tests of General Relativity and the refinement of satellite orbital dynamics modeling.

Keywords orbital perturbation, earth tide, satellite laser ranging, frame-dragging effect

1. Introduction

Frame-dragging, also known as the Lense-Thirring effect, is a fundamental phenomenon predicted by Einstein's theory of General Relativity (Lense and Thirring 1918). It describes how a rotating massive body, such as Earth, drags the surrounding spacetime structure, inducing a tiny precession in the orbits of nearby test bodies. This effect holds significant theoretical importance for understanding astrophysical processes, including the dynamics of rotating black holes.

Satellite Laser Ranging (SLR) to dedicated satellites, such as the two LAGEOS and the two LARES satellites, has been the primary method for the experimental verification of this effect. I. Ciufolini first proposed a novel method in 1986 to measure the effect using a pair of satellites with supplementary orbital parameters (Ciufolini 1986). Building on this, Ciufolini and his collaborators reported the first direct measurement of the Earth's spin-induced Lense-Thirring effect in 1997, using laser-ranging data from the LAGEOS satellites (Ciufolini et al. 1997). This work was preceded by and built upon their preliminary orbital analysis in 1996 (Ciufolini and Wheeler 1996).

Subsequently, through continuous refinement of Earth’s gravity field models and the development of multi-satellite combination techniques, the team has progressively enhanced the measurement accuracy. For instance, by analyzing long-term data from LAGEOS and LAGEOS 2, Ciufolini and Pavlis achieved a measurement accuracy at the level of approximately 10% in 2004 (Ciufolini and Pavlis 2004). With the inclusion of the dedicated satellite LARES, the research goal was further directed towards a 1% measurement accuracy (Ciufolini et al. 2017). Currently, the new observational system based on the satellites LARES 2 and LAGEOS aims to push the verification accuracy into the novel sub-percent regime (Ciufolini et al. 2024).

The core challenge in achieving this precise measurement lies in the extreme weakness of the Lense-Thirring signal, which is several orders of magnitude smaller than the classical Newtonian perturbations such as those from Earth’s oblateness (e.g., the J_2 term). Therefore, the key to high-precision verification is the extremely accurate modeling and precise subtraction of various classical orbital perturbations, including Earth’s static and time-varying gravitational field, tidal perturbations, and non-conservative force effects. Among these, the effective control of errors in Earth’s gravity field models, particularly the higher-degree even zonal harmonics, is one of the decisive factors in improving verification accuracy. This study investigates the perturbations of Earth tides on the orbital nodes and inclinations of the LARES 2 and LAGEOS satellites, which employ a distinctive “butterfly” orbital configuration: their semi-major axes are comparable, orbits are nearly circular (near-zero eccentricities), and inclinations are complementary—LARES 2 follows a prograde orbit with $i_{LARES\ 2}=70.165^\circ$, while LAGEOS is in a retrograde orbit with $i_{LAGEOS}=109.8469^\circ$ (Ciufolini et al. 2023). This property enables effective cancellation of the J_2 -related precession when combining the nodal signals of the two satellites, while simultaneously enhancing the Lense-Thirring effect signals. This separation of the relativistic signal from Earth’s oblateness-driven precession is critical for achieving high-precision measurements.

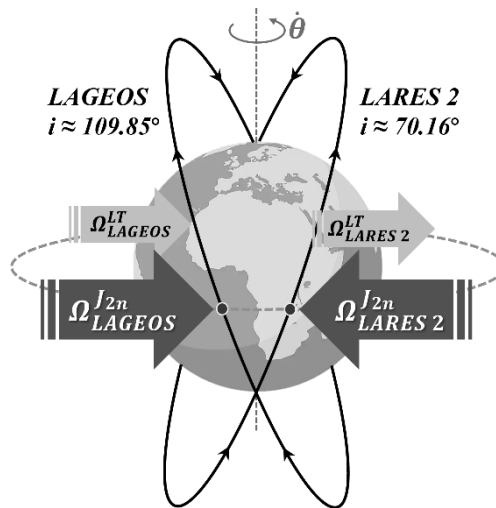


Fig. 1 The “butterfly-shaped” orbital configuration of LAGEOS and LARES 2.

However, because the two satellites’ orbital inclinations are not strictly supplementary and have different time-varying characteristics, the above cancellation is incomplete. After the largest Earth oblateness perturbation is canceled, quantitative analysis of uncanceled classical perturbations becomes key to improving accuracy. For example, time-varying perturbation sources like Earth tides cause complex and unsynchronized, asymmetric periodic changes in the orbital elements of the two satellites.

This is an essential difference in geodynamic response between prograde and retrograde orbits, meaning that even under the same order of Earth tidal effects, the perturbation periods and amplitudes experienced by the two satellites are not identical. To use an analogy, imagine two runners with different constant speeds circling a standard running track. The time interval between their meetings will be significantly different depending on whether they run in the same direction or opposite directions. The observed frequency of tidal perturbations acting on the satellite is modulated by both satellite orbital motion and the intrinsic tidal frequencies—in addition to the inherent frequencies of tidal-generating bodies (Sun, Moon), there are combination terms involving the satellite nodal precession and Earth’s rotation (see Equation 10) $m(\dot{\Omega} - \dot{\theta})$. Since LARES 2 and LAGEOS have opposite signs in $\dot{\Omega}$, even for the same Doodson number-defined tide (i.e., same $\sum_{i=1}^6 \frac{2\pi J_i}{\gamma_i}$), their perturbation frequencies

$\dot{\Gamma}_{jlm}^p$ will differ due to the term $m(\dot{\Omega} - \dot{\theta})$, leading to different perturbation periods, for harmonic signals, once their periods are different, they cannot cancel each other out through linear combination.

In summary, precise calculation of tidal perturbations on LARES 2 and LAGEOS individually is not only fundamental to understanding the time-varying characteristics of their orbital inclinations but also necessary for further separating Earth oblateness precession from frame-dragging and improving geodetic experiment accuracy.

This study will obtain perturbation periods and amplitudes of different order modes on the orbital nodes and inclinations of LARES 2 and LAGEOS by selecting specific tidal modes, thereby avoiding computational complexity caused by high-frequency variations in satellite argument of pericenter and mean anomaly. Additionally, we will quantitatively assess the cumulative impact of the secondary tidal constituents that are filtered out in the selection process. This comprehensive analysis provides important support for in-depth study of satellite orbital dynamics and high-precision verification of the Lense-Thirring effect.

The precision modeling of Earth tides remains a critical factor in high-precision satellite laser ranging (SLR) measurements, particularly for missions such as LAGEOS and LARES. While early Earth tide models typically accounted only for the dominant tidal constituents, this simplified approach has become insufficient as measurement accuracies have reached the sub-centimeter level. Studies by Gurzadyan et al. (2017) and Gurzadyan et al. (2025) identified 110 significant Earth tide constituents that affect the orbits of LARES and LARES 2, thereby capturing finer tidal effects; however, the specific reasons or mechanisms behind this selection were not explicitly discussed.

In this context, our study adopts a new perspective. We first compute the perturbation periods and amplitudes for 402 Earth tide constituents on the orbital nodes and inclinations of LAGEOS and LARES 2, based on the tidal list provided by the convention of Cartwright and Tayler (1971). Subsequently, we apply a filtering threshold derived from the current SLR orbit determination accuracy to isolate the most significant constituents. It is noteworthy that the minor constituents—those filtered out due to their relatively weak amplitudes—often have closely spaced frequencies. Consequently, they may coherently add in the time domain, potentially resulting in a cumulative impact that is non-negligible.

Therefore, the primary objective of this study is to evaluate whether these minor constituents can indeed be neglected. Moreover, we aim to provide reasonable recommendations for the existing “individual constituent filtering” methodology, thereby offering crucial support for the in-depth study of satellite orbital dynamics and the high-precision verification of the Lense-Thirring effect.

2. Tidal Perturbations

2.1 Earth tides

2.1.1 Earth as the intermediate link: tidal response and perturbation transfer to satellites

The Earth’s spatial tidal potential V_T is expressed via time variations of Stokes coefficients C_{lm} and S_{lm} in the spherical harmonic expansion of Earth’s gravitational potential (Melchior 1983; Eanes 1983; Sanchez 1975). This arises because tide-generating bodies (primarily the Moon and Sun) lie far farther from Earth’s center of mass than Earth’s radius—thus, Earth’s response to the external potential is linear, with the additional potential from Earth’s shape deformation proportional to the external potential.

This study employs the linear perturbation formulation of Kaula (1966), using the tidal potential V_T (minus) as a “disturbing function” to evaluate the changes in the orbital elements, specifically the right ascension of the ascending node (and the inclination), via Lagrange’s planetary equations.

For the Earth’s gravitational potential V :

$$V = -GM \sum_{l=2}^{\infty} \sum_{m=0}^l R^l V_{lm} \quad (1)$$

where G is the gravitational constant, M and R are the mass and mean equatorial radius of Earth, respectively, and V_{lm} are the components of the gravitational potential at different degrees l and orders m , with the form Kaula (1966):

$$V_{lm} = \frac{1}{a^{l+1}} \sum_{p=0}^l F_{lmp}(i) \sum_{q=-\infty}^{+\infty} G_{lpq}(e) \left[\begin{pmatrix} C_{lm} \\ -S_{lm} \end{pmatrix}_{l-m \text{ odd}}^{l-m \text{ even}} \cos(\psi_{lmpq}) + \begin{pmatrix} S_{lm} \\ C_{lm} \end{pmatrix}_{l-m \text{ odd}}^{l-m \text{ even}} \sin(\psi_{lmpq}) \right] \quad (2)$$

where:

- C_{lm} , S_{lm} are the normalized, dimensionless Stokes coefficients of Earth's gravitational potential;
- $F_{lmp}(i)$, $G_{lpq}(e)$: the inclination and eccentricity functions, respectively (Kaula 1961; 1964; 1966);
- p , q are the expansion indices for the inclination and eccentricity functions, the "decomposition indices of the response end (satellite orbit)", which resolve the adaptation modes of orbital inclination and eccentricity to the gravitational perturbation.
- $\psi_{lmpq} = m(\Omega - \theta) + (l - 2p)\omega + (l - 2p + q)\mu$, where θ is the local sidereal time (Bertotti and Carpino 1989);
- a , e , i , Ω , ω , μ are the six unperturbed Keplerian orbital elements of the satellite (semi-major axis, eccentricity, inclination, right ascension of the ascending node, argument of perigee, and mean anomaly), respectively.

Expressing V_{lm} as a function of orbital elements in an inertial frame (not Earth's precessing spherical coordinates (r, ϕ, λ)) enables direct "perturbation source-orbital response" modeling. This allows V_{lm} to be used directly as the disturbing function in Lagrange's equations, avoiding complexity from reference frame dynamics (e.g., precession/nutation time-variability) or coordinate transformations—critical for efficient, accurate tidal effect analysis (e.g., in the calculation of $\Delta\Omega_{lmpq}$ and Δi_{lmpq}).

According to Kaula's theory, for an external body of mass M^* with orbital elements $X^* = (a^*, e^*, i^*, \Omega^*, \omega^*, \mu^*)$ in the Earth's inertial coordinate system, the tidal potential component of degree l, m generated by it at a spatial point (r, ϕ, λ) can be written as (Efroimsky and Williams 2009):

$$V_{lm}^*(r, \phi, \lambda; X^*) = \frac{GM^*}{a^*} \left(\frac{R}{a^*}\right)^l \frac{(l-m)!}{(l+m)!} (2 - \delta_{0m}) P_{lm}(\sin\phi) \times \sum_{p=0}^l F_{lmp}(i^*) \sum_{q=-\infty}^{+\infty} G_{lpq}(e^*) \begin{pmatrix} \cos \\ \sin \end{pmatrix}_{l-m \text{ odd}}^{l-m \text{ even}} (\psi_{lmpq}^* - m\lambda) \quad (3)$$

where $P_{lm}(\sin\phi)$ is the normalized Legendre function, and ψ_{lmpq}^* is determined by the Keplerian orbital elements of the tide-generating body:

$$\psi_{lmpq}^* = m(\Omega^* - \theta) + (l - 2p)\omega^* + (l - 2p + q)\mu^* \quad (4)$$

For Earth's response to the aforementioned tidal potential, linear tidal theory uses Love numbers k_{lm} (Love 1926; Petit and Luzum 2010)—intrinsic elastic Earth parameters quantifying gravitational potential/deformation response to external forcing. At the satellite's position (r, ϕ, λ) , the additional gravitational potential from Earth's tidal deformation is:

$$V_{T,S} = - \sum_{l=2}^{+\infty} \sum_{m=0}^l k_{lm} \left(\frac{R}{r}\right)^{l+1} V_{lm}^*(r, \phi, \lambda; X^*) \quad (5)$$

The key point here is that the response potential $V_{T,S}$ is proportional to the values of the tidal potential V_{lm}^* at and outside Earth's surface ($r \geq R$), and attenuates according to $\left(\frac{R}{r}\right)^{l+1}$, with the Love numbers k_{lm} quantifying the magnitude of this response.

Since the additional gravitational potential is the deformation potential of Earth under the gravitational forces of the Sun and Moon, it must be referenced to Earth's center of mass, and satellite orbital perturbation analysis uses an inertial frame, Kaula's transformation is applied again to expand $P_{lm}(\sin \phi)$ using $F_{lmp}(i)$ and $G_{lpq}(e)$. This eliminates ϕ , λ and converts $V_{T,S}$ to the geocentric inertial frame. After index rearrangement, the disturbing function becomes:

$$V_{T,S} = -\frac{GM^*}{a^*} \sum_{l=2}^{+\infty} \sum_{m=0}^l k_{lm} \left(\frac{R}{a}\right)^{l+1} \left(\frac{R}{a^*}\right)^l \frac{(l-m)!}{(l+m)!} (2 - \delta_{0m}) \sum_{h=0}^l F_{lmh}(i^*) \sum_{j=-\infty}^{+\infty} G_{lhj}(e^*) \sum_{p=0}^l F_{lmp}(i) \times \sum_{q=-\infty}^{+\infty} G_{lpq}(e) \cos(\psi_{lmhj}^* + \psi_{lmpq} - \epsilon_{lmhj}) \quad (6)$$

where $\epsilon_{lmhj} = \dot{\psi}_{lmhj}^* \Delta t_{lmhj}$, which represents the linear variation of the solar-lunar phase with time. $\dot{\psi}_{lmhj}^*$ is the angular frequency of the tidal component, which is the first derivative of equation (4) with respect to time (denoted later by σ to distinguish from the satellite's angular frequency); Δt_{lmhj} is the time difference from Earth's interior anelasticity. Furthermore, $\psi_{lmpq} = m(\Omega - \theta) + (l - 2p)\omega + (l - 2p + q)\mu$, where the physical meaning of the symbols here are similar to those in equation (4), except that it refers to the perturbed body, i.e., the artificial satellite. The expressions for the inclination functions $F_{lmp}(i)$ and eccentricity functions $G_{lpq}(e)$ of various degrees and orders used in this paper are shown in Table 1. The expressions for $F_{lmp}(i)$ and $G_{lpq}(e)$ differ for distinct values of l , m , p , and q . Specifically, the expressions $F_{201}(i) = \frac{3}{4} \sin^2 i - \frac{1}{2}$, $F_{211}(i) = -\frac{3}{2} \sin i \cos i$, $F_{211}(i) = \frac{3}{2} \sin^2 i$, and $G_{210}(e) = \frac{1}{\sqrt{(1-e^2)^3}}$ are adopted in this paper when calculating the perturbations of the 2nd-degree earth tides on LAGEOS and LARES 2. The expressions under other conditions are listed in Tables 1 and 2 of Kaula (1966).

2.1.2 Frequency-dependent response of earth

The preceding derivation of the expression for the gravitational potential of Earth's tides (Equation 6) adopted an idealized frequency-independent assumption for the Love numbers. However, the tidal response of the actual Earth exhibits significant frequency dependence: anelasticity of the mantle leads to phase lag in tidal deformation, and this effect varies with the tidal frequency band (e.g., long-period, diurnal, semidiurnal) (Wahr and Bergen 1986; Petit and Luzum 2010); meanwhile, resonance effects from Earth's rotation, oblateness, and Free Core Nutation (FCN) significantly modulate the Love number values. Ignoring this frequency dependence would lead to modeling errors in the amplitudes of tidal perturbations for different frequency bands, which in turn would affect the extraction of the frame-dragging effect at sub-percent level accuracy.

To precisely quantify this characteristic, it is necessary to introduce frequency-dependent astronomical amplitudes $H_l^m(f)$ and Love numbers $k_{lm}(f)$. The astronomical amplitudes (Cartwright and Tayler 1971; Cartwright and Edden 1973) are obtained by analyzing ephemerides to determine the contribution of the tidal potential's equivalent tide height for different frequencies f . The frequency-dependent Love numbers $k_{lm}(f)$ are constructed by strictly adhering to the layered modeling framework of IERS Conventions 2010: the basic elastic parameters are derived from the elliptical, rotating, non-oceanic version of the Preliminary Reference Earth Model (PREM) (Dziewonski and Anderson 1981)—a foundational setup for body tide modeling first formalized by Wahr (1981), who explicitly incorporated Earth's ellipticity and rotation into tidal Love number calculations; the frequency response due to mantle anelasticity is quantified using the mantle Q model of Widmer et al. (1991)

in conjunction with the power-law relationship of Wahr and Bergen (1986); resonance effects for diurnal tides are addressed using the nutation-wobble coupling model of Mathews et al. (2002), which incorporates corrections for the resonance frequencies (σ_α) and coefficients (L_α) of the Chandler wobble, Free Core Nutation (FCN), and Free Inner Core Nutation (FICN), as Equation 7 shows; and the frequency-dependent contribution of ocean tide loading is converted into corrections for the body tide Love numbers via the equivalent model of Wahr and Sasao (1981), with ocean tide data sourced from the FES2004 model (Lyard et al. 2006). The coupled application of these models ensures the computational accuracy of both the real part (amplitude) and the imaginary part (energy dissipation) of the Love numbers across different tidal frequency bands (long-period, diurnal, and semidiurnal).

$$\begin{cases} k_{21}^{(0)}(f) = k_{21}^{(0)} + \sum_{\alpha=1}^3 \frac{L_\alpha}{\sigma - \sigma_\alpha} \\ \sigma = f / (15 \times 1.002737909) \end{cases} \quad (7)$$

Figure 2 is a comparative diagram of the frequency-dependent tidal perturbations (see in 2.1.5 and Appendix Table 1) and frequency-independent tidal perturbations (nominal love numbers for each degree and order are referred to Petit and Luzum (2010) on the node of LARES 2, and it can be observed from Figure 2(b) that the amplitude difference between the two is considerable, reaching up to 322 mas—which is more than ten times the frame-dragging effect—thus, it is essential to take into account the frequency-dependent response of the Earth tides when calculating satellite orbit perturbations.

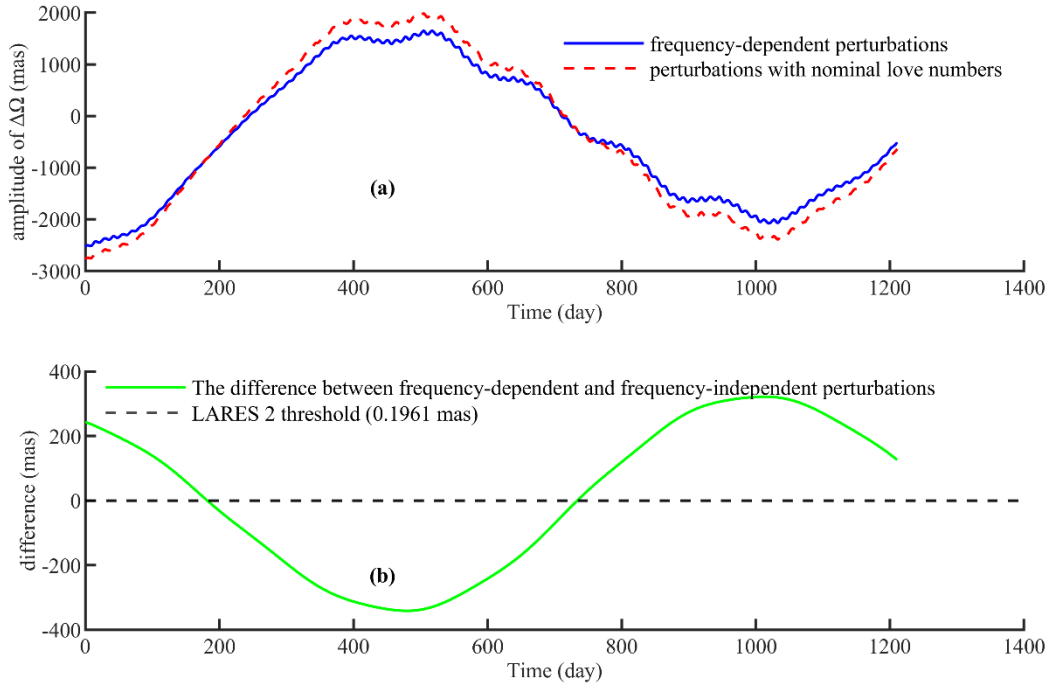


Fig. 2 Comparison of tidal perturbation time series on node of LARES 2: frequency-dependent and nominal love numbers.

Based on this, the term in Equation 6 related to the tide-generating body, $\frac{GM^*}{a^*} \left(\frac{R}{a^*}\right)^l$ must be transformed into a standard form that includes frequency information, with the specific substitution as $\frac{GM^*}{a^*} \left(\frac{R}{a^*}\right)^l = gN_{lm} H_l^m(f)$.

$g = \frac{GM}{R^2}$ is the acceleration of gravity at Earth's surface. $H_l^m(f)$ is proportional to $(M^*/M)(R/a^*)^l$, with dimensions of L , and it incorporates the inclination functions $F_{lmh}(i^*)$ and eccentricity functions $G_{lmj}(e^*)$ of the tide-generating body.

In tidal theory, the tidal potential at Earth's surface is proportional to the product of the surface gravity acceleration and the equivalent tide height, i.e., $gH_l^m(f)$, and the spherical harmonic normalization coefficient $N_{lm} = \sqrt{\frac{(2l+1)(l-m)!}{4\pi(l+m)}}$ originates from spherical harmonic theory, without it, the amplitudes of different l, m components cannot be directly compared.

In summary, the additional gravitational potential due to Earth's tidal deformation, which perturbs an artificial satellite, is expressed as:

$$V_{T,S} = -g \sum_{l=2}^{+\infty} \left(\frac{R}{a}\right)^{l+1} \sum_{m=0}^l N_{lm} \times \sum_{p=0}^l F_{lmp}(i) \sum_{q=-\infty}^{+\infty} G_{lpq}(e) \sum_f H_l^m(f) k_{lm}(f) \cos(\sigma t + \psi_{lmpq} - \epsilon_{lm}(f)) \quad (8)$$

where $\sigma = 2\pi f$ is the angular frequency of the tidal component of the tide-generating body (satisfying $\sigma = 2\pi/P$ with period P), which is a combination angle variable composed of the orbital elements of the tide-generating body. To efficiently and standardly encode all frequency components, Doodson numbers are used as coefficients for the corresponding linear combination of the angular frequencies of the tide-generating body, with the expression given by Equation 9. $\epsilon_{lm}(f)$ represents the phase lag of the Earth tide for degree order l, m and frequency σ , caused by the anelasticity of the Earth's mantle, and can be treated as a time-invariant quantity in this study.

$$\sigma = j_1 \dot{t} + j_2 \dot{s} + j_3 \dot{h} + j_4 \dot{p} + j_5 \dot{N}' + j_6 \dot{p}_s \quad (9)$$

Here, $j_1 \sim j_6$ are the Doodson numbers (Doodson 1921) that define the tidal components; for example, j_1 is used to distinguish the types of tides: $j_1 = 1$ for long-period/zonal tides, $j_1 = 1$ for diurnal/tesseral tides, and $j_1 = 2$ for semidiurnal/sectorial tides. \dot{t} , \dot{s} , \dot{h} , \dot{p} , \dot{N}' and \dot{p}_s are respectively the rate of change of the lunar mean time, the Moon's mean longitude, the Sun's mean longitude, the Moon's mean longitude of perigee, the Moon's mean longitude of the ascending node, and the Sun's mean longitude of perigee.

These six fundamental astronomical angular frequencies can be expressed as $\alpha_i = \{347.80925061, 13.17639673, 0.98564734, 0.11140408, 0.05295392, 0.00004707\}$ (\circ/day), with their corresponding periods being $\gamma_i = 360/\alpha_i$ (days). Thus, $\sigma = \sum_{i=1}^6 \frac{2\pi j_i}{\gamma_i}$.

For the time variation of the phase term $\sigma t + \psi_{lmpq} - \epsilon_{lm}(f)$, it should be noted that ψ_{lmpq} is also a time-varying quantity, which can be written as $[m(\dot{\Omega} - \dot{\theta}) + (l-2p)\dot{\omega} + (l-2p+q)\dot{\mu}]t$. Therefore, this phase can be expressed as $[\sigma + m(\dot{\Omega} - \dot{\theta}) + (l-2p)\dot{\omega} + (l-2p+q)\dot{\mu}]t - \epsilon_{lm}(f) = \dot{\Gamma}_{j_{lmp}} t - \epsilon_{lm}(f)$. Taking the first derivative with respect to time of the phase term yields the frequency of the tidal perturbation (Bertotti and Carpino 1989):

$$\dot{\Gamma}_{j_{lmp}} = \sum_{i=1}^6 \frac{2\pi j_i}{\gamma_i} + m(\dot{\Omega} - \dot{\theta}) + (l-2p)\dot{\omega} + (l-2p+q)\dot{\mu} \quad (10)$$

2.1.3 Screening of perturbation modes

This study focuses on large-amplitude long-period perturbations: they require modeling, while short-period ones (negligible amplitude) average to zero over a full satellite orbit. That is, only the case where $l-2p+q=0$ is considered.

Secondly, to more comprehensively consider tidal perturbations with amplitudes within the observable range, in addition to focusing on the “source” of the astronomical amplitude of each tide—that is, calculating only the case when $l=2$ we also need to examine the eccentricity function: for the case where $q=0$, $G_{lpq}(e) \approx 1$, and the perturbation amplitude is not excessively scaled, thus requiring key consideration; for the case where $q \neq 0$, $G_{lpq}(e) \approx 0$, and the perturbation amplitude also becomes negligible, therefore this study does not consider it. In summary, this study focuses on the mode where $(l, p, q) = (2, 1, 0)$. At this time, the tidal perturbation frequency simplifies to:

$$\dot{\Gamma}_{j,lmq} = \sum_{i=1}^6 \frac{2\pi j_i}{\gamma_i} + m \left(\dot{\Omega} - \frac{2\pi}{\gamma_{1+2}} \right) = \sum_{i=1}^6 \frac{2\pi j_i}{\gamma_i} + m \left(\dot{\Omega} - \frac{2\pi}{360/(\alpha_1 + \alpha_2)} \right) \quad (11)$$

Notably, incorporating other planets’ tidal effects when deriving Earth tide gravitational potential would boost precision but increase complexity. Given their weak effects and the sharp rise in computational cost for tidal potential expansion, these effects are temporarily excluded here.

2.1.4 Derivation of the tidal perturbation expression

Tidal perturbations originate from conservative gravitation, and in Lagrangian perturbation theory, the disturbing function \mathcal{R} is the potential energy function of conservative forces; the tidal potential, as the potential function of tidal gravitation, is physically consistent with \mathcal{R} , therefore in Lagrange’s equations, the tidal potential (minus) can replace \mathcal{R} to analyze the perturbations of tides on satellite orbits:

$$\frac{d\Omega}{dt} = \frac{1}{\sqrt{GMa(1-e^2)} \sin i} \frac{\partial \mathcal{R}}{\partial i} = - \frac{1}{\sqrt{GMa(1-e^2)} \sin i} \frac{\partial V_{T,S}}{\partial i} \quad (12)$$

By integrating the instantaneous rate of change of the right ascension of the ascending node $\frac{d\Omega}{dt}$ over time, the cumulative perturbation $\Delta\Omega_{lmq}$ can be obtained (Kaula 1966; Bertotti and Carpino 1989):

$$\Delta\Omega_{lmq} = \int \frac{d\Omega}{dt} dt = \frac{1}{\sin i} \sqrt{\frac{GMR^{2l-2}}{a^{2l+3}(1-e^2)}} \frac{\partial F_{lmq}(i)}{\partial i} G_{lpq}(e) N_{lm} \frac{H_l^m(f) k_{lm}(f)}{\dot{\Gamma}_{j,lmq}} \sin(\dot{\Gamma}_{j,lmq} t - \epsilon_{lm}(f)) \quad (13)$$

It can be seen that the cumulative perturbation $\Delta\Omega_{lmq}$ is a quasi-trigonometric function. To obtain its amplitude, the maximum value of 1 is taken for $\sin(\dot{\Gamma}_{j,lmq} t - \epsilon_{lm}(f))$, yielding the amplitude:

$$\Delta\Omega_{lmq} = \frac{1}{\sin i} \sqrt{\frac{GMR^{2l-2}}{a^{2l+3}(1-e^2)}} \frac{\partial F_{lmq}(i)}{\partial i} G_{lpq}(e) N_{lm} \frac{H_l^m(f) k_{lm}(f)}{\dot{\Gamma}_{j,lmq}} \quad (14)$$

Similarly, the perturbation period of Earth tides on the orbital inclination is consistent with that on the right ascension of the ascending node, and the derivation of the perturbation amplitude is also analogous, with the only difference being in the Lagrange equations used. The tidal perturbations on other orbital elements can be derived in the same manner, and will not be elaborated further in this paper.

$$\frac{di_{lmq}}{dt} = \frac{1}{\sqrt{GMa(1-e^2)} \sin i} \left(\cos i \frac{\partial V_{T,S}}{\partial \omega} - \frac{\partial V_{T,S}}{\partial \Omega} \right) \quad (15)$$

Here, the derivation process is omitted and the result is given directly:

$$\Delta i_{lmq} = \frac{[\cos i (l-2p) - m]}{\sin i} \sqrt{\frac{GMR^{2l-2}}{a^{2l+3}(1-e^2)}} F_{lmq}(i) G_{lpq}(e) N_{lm} \frac{H_l^m(f) k_{lm}(f)}{\dot{\Gamma}_{j,lmq}} \quad (16)$$

The orbital elements of LARES 2 and LAGEOS satellites used in the calculations are shown in Table 1, including the mean orbital inclination, mean semi-major axis, mean eccentricity (Ciufolini et al. 2023), nodal precession period $P(\Omega)$ — with the $P(\Omega)$ of both satellites being 1050 days as suggested by Ciufolini. These mean orbital elements cover a 127-day observation period from July 13, 2022, to November 16, 2022, and derived from SLR observations processed by the GEODYN II and UTOPIA orbit estimators.

Table 1 The orbital elements of LARES 2 and LAGEOS

	Inclination (degrees)	mean semi-major axis (km)	mean eccentricity	P(Ω) (day)
LARES 2	70.1615	12266.1359395	0.00027	-1050
LAGEOS	109.8469	12270.020705	0.00403	1050

As for the calculation of the instantaneous phase of tidal perturbations, it is actually simpler. The essence is the superposition result of the dynamic accumulation of astronomical angles of tide-generating bodies and satellite orbital arguments with the phase lag of Earth's anelastic response. Its core physical significance is: at the target epoch, the tidal disturbance signal of tide-generating bodies on Earth, after being modulated by Earth's anelasticity, acts on the instantaneous phase state of the satellite orbit, that is, "absolute astronomical benchmark (such as J2000.0 epoch) + time evolution part + satellite relative orbital benchmark (first observation moment) + time evolution part + geophysical response (anelastic lag)", to ensure high precision and reproducibility of the phase. Among them, the Earth lag response part is the arctangent of the ratio of the imaginary part to the real part of the Love number.

2.1.5 Results

For the 402 perturbations of earth tides (392 2-nd degree tides and 10 3-rd degree tides) to the orbits of LARES 2 and LAGEOS, their perturbation periods and amplitudes are detailed in Appendix Table 1. To identify significant tidal perturbation modes from these, it is necessary to set a threshold based on the orbit determination accuracy of the two satellites. Specifically, the threshold should refer to the intrinsic property of satellite orbit determination — i.e., the minimum resolvable capability of orbit solutions achievable with existing observational data and orbit determination methods (corresponding to internal consistency accuracy), rather than the observed fitting residuals containing biases from various physical perturbation models (corresponding to external consistency accuracy). The observed fitting residuals reflect the actual effect of implementing the model into orbit solutions; this indicator is used to evaluate the deviation adaptability between various physical perturbation models and actual observations, which is thus not suitable as a criterion for screening tidal perturbation modes. Based on this, this study adopts the RMS of overlap orbit differences for LAGEOS and LARES 2 (Shao et al. 2025).

For LAGEOS, the RMS of overlap orbit differences in the tangential (T) Δr_t and normal (N) directions Δr_n are 2.16 cm and 1.34 cm, respectively, from which the corresponding uncertainties in the orbital inclination (Δi_{un}) and the node ($\Delta \Omega_{un}$) are derived as 0.2253 mas and 0.2451 mas via Equation 17. For LARES 2, the mean RMS values of overlap orbit differences in the T and N directions are smaller (1.35 cm for Δr_t and 1.14 cm for Δr_n , respectively) due to its favorable orbital and structural characteristics; correspondingly, Δi_{un} and $\Delta \Omega_{un}$ are 0.1917 mas and 0.1961 mas, respectively. A tidal perturbation mode was retained if either its Δi_{un} or $\Delta \Omega_{un}$ amplitude exceeded the threshold for the corresponding satellite. These values were adopted as a threshold to identify 83 significant tidal perturbation modes (81 2-nd degree tides and 2 3-rd degree tides). The perturbation periods and amplitudes for these selected modes are presented in Tables 2~4.

$$\left\{ \begin{array}{l} \Delta \Omega_n = \frac{1}{a} \Delta r_n \sin i \\ \Delta \Omega_t = \frac{1}{a} \Delta r_t \cos i \\ \Delta \Omega_{un} = \frac{1}{a} \sqrt{\Delta \Omega_n^2 + \Delta \Omega_t^2} \\ \Delta i_{un} = \frac{\Delta r_n}{a} \end{array} \right. \quad (17)$$

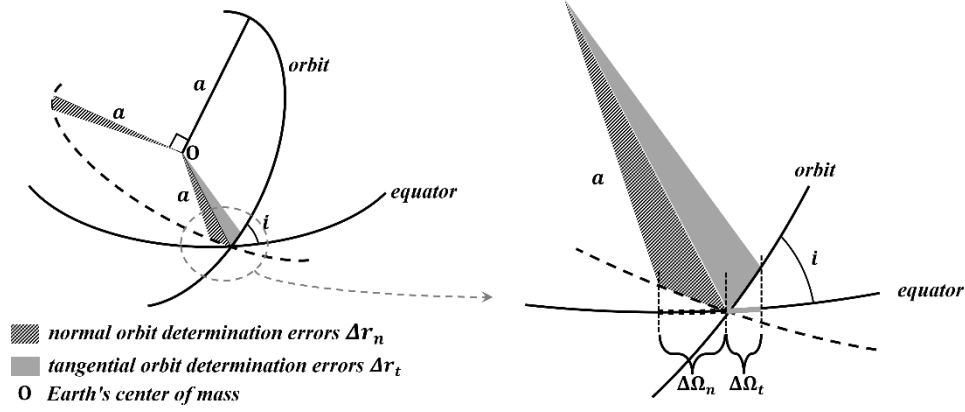


Fig. 3 Schematic diagram of the contribution of satellite orbital normal and tangential errors to the node and inclination

Table 2 Perturbation periods and amplitudes of the right ascension of the ascending node and orbital inclination for LAGEOS and LARES 2 satellites ($l=2, m=0, p=1, q=0$)

Tide name	Doodson number	Love number	H_l^m (m)	Perturbation periods (days)		$\Delta\Omega_{lmpq}$ (mas)		Δi_{lmpq} (mas)	
				LAGEOS	LARES 2	LAGEOS	LARES 2	LAGEOS	LARES 2
	055.565	0.315416	0.02793	6798.3636	6798.3636	-1073.8847	1074.6041	0	0
	055.575	0.313178	-0.00027	3399.1818	3399.1818	5.1538	-5.1573	0	0
S_a	056.554	0.307390	-0.00492	365.2596	365.2596	9.9050	-9.9117	0	0
S_{sa}	057.555	0.305946	-0.031	182.6211	182.6211	31.0568	-31.0776	0	0
	057.565	0.305896	0.00077	177.8438	177.8438	-0.7511	0.7516	0	0
	058.554	0.305174	-0.00181	121.7493	121.7493	1.2058	-1.2067	0	0
M_{sm}	063.655	0.302920	-0.00673	31.8119	31.8119	1.1629	-1.1637	0	0
	065.445	0.302709	0.00231	27.6667	27.6667	-0.3469	0.3471	0	0
M_m	065.455	0.302709	-0.03518	27.5546	27.5546	5.2615	-5.2651	0	0
	065.465	0.302699	0.00229	27.4433	27.4433	-0.3411	0.3413	0	0
	065.655	0.302679	0.00188	27.0925	27.0925	-0.2764	0.2766	0	0
M_{sf}	073.555	0.301818	-0.00583	14.7653	14.7653	0.4659	-0.4662	0	0
	075.355	0.301728	-0.00288	13.7773	13.7773	0.2147	-0.2148	0	0
M_f	075.555	0.301718	-0.06663	13.6608	13.6608	4.9243	-4.9276	0	0
	075.565	0.301718	-0.02762	13.6334	13.6334	2.0372	-2.0385	0	0
M_{tm}	085.455	0.301197	-0.01276	9.1329	9.1329	0.6294	-0.6298	0	0
	085.465	0.301197	-0.00529	9.1207	9.1207	0.2606	-0.2607	0	0

The periods of zonal tides are determined solely by the orbital motion of the Sun and Moon, and are identical for both LAGEOS and LARES 2 satellites, with calculation results shown in Table 2. The typical characteristics of these tidal periods are: an 18.6-year (6798.3636 days) period associated with the regression of the Moon's nodes, and a half-year (182.6211 days) period associated with the variation in the Sun's declination. Their values depend on the long-term orbital parameters of the Sun and Moon, (such as the lunar nodal regression period and the annual solar motion).

For zonal tides, the perturbation amplitudes on the ascending nodes of LAGEOS and LARES 2 are nearly equal in magnitude but opposite in sign, whereas their perturbation amplitudes on orbital inclination are zero. This results

from the axial symmetry of Earth's deformation induced by zonal tides: at a given latitude, solid-Earth uplift or subsidence and ocean mass redistribution are identical for all longitudes and thus do not depend on the right ascension of the ascending node. Consequently, in Equation 15, $\frac{\partial T_{T,S}}{\partial \Omega} = 0$, and with $l-2p=0$, the result of integrating $\frac{di_{lmpq}}{dt}$ over time is zero. This agrees with the conclusion of Bertotti and Carpino (1989) that “zonal tides ($m=0$) cancel out due to symmetry”.

However, due to differences in data recency, the numerical results in this study differs from those in the 1989 report by approximately 1%-20%. At that time, LARES 2 had not yet been launched, and its orbital parameters were simulated based on LAGEOS, whereas today several years of laser-ranging observations are available for LARES 2, directly affecting amplitude estimates (for example, the semi-major axis differs by about 4 km). In addition, the Love numbers used in 1989 adopted a uniform value of $k_2 = 0.317$, ignoring frequency dependence. In contrast, the present work employs frequency-dependent Love numbers constrained by observational studies of Earth's internal structure (e.g., mantle viscosity), providing a more realistic representation of Earth's tidal response. Similar differences apply to the cases following.

Table 3 Perturbation periods and amplitudes of the right ascension of the ascending node and orbital inclination for LAGEOS and LARES 2 satellites ($l=2, m=1, p=1, q=0$)

Tide name	Doodson number	Love number	$H_l^m(m)$	Perturbation periods		$\Delta\Omega_{lmpq}$ (mas)		Δi_{lmpq} (mas)	
				LAGEOS	LARES 2	LAGEOS	LARES 2	LAGEOS	LARES 2
2Q ₁	125.755	0.298013	-0.00664	-6.9045	-6.8149	0.2410	0.2382	-0.1000	0.0988
σ_1	127.555	0.298003	-0.00802	-7.1441	-7.0482	0.3012	0.2975	-0.1250	0.1234
	135.645	0.297853	-0.00947	-9.2006	-9.0421	0.4577	0.4504	-0.1900	0.1868
Q ₁	135.655	0.297843	-0.05020	-9.2131	-9.0542	2.4297	2.3908	-1.0084	0.9916
ρ_1	137.455	0.297813	-0.00954	-9.6446	-9.4707	0.4833	0.4752	-0.2006	0.1971
	145.545	0.297483	-0.04946	-13.8127	-13.4586	3.5847	3.4972	-1.4877	1.4505
O ₁	145.555	0.297473	-0.26221	-13.8409	-13.4853	19.0422	18.5766	-7.9028	7.7050
τ_1	147.555	0.297393	0.00343	-14.9759	-14.5605	-0.2694	-0.2623	0.1118	-0.1088
$N_{\tau 1}$	153.655	0.296623	0.00194	-24.5007	-23.4083	-0.2487	-0.2379	0.1032	-0.0987
L_{k1}	155.455	0.296363	0.00741	-27.8101	-26.4111	-1.0772	-1.0243	0.4471	-0.4249
N_{O1}	155.655	0.296333	0.02062	-28.2971	-26.8499	-3.0498	-2.8975	1.2657	-1.2018
	155.665	0.296323	0.00414	-28.4154	-26.9564	-0.6149	-0.5840	0.2552	-0.2422
χ_1	157.455	0.295993	0.00394	-32.8059	-30.8765	-0.6748	-0.6359	0.2801	-0.2638
π_1	162.556	0.289961	-0.00714	-137.7180	-109.0991	5.0290	3.9890	-5+2.0871	1.6545
	163.545	0.287131	0.00137	-214.1084	-152.0845	-1.4856	-1.0566	0.6165	-0.4382
P ₁	163.555	0.286921	-0.12203	-221.0708	-155.5646	136.5268	96.1938	-56.6609	39.8982
	164.554	0.280660	0.00103	-560.0173	-270.9718	-2.8555	-1.3834	1.1851	-0.5738
S ₁	164.556	0.280660	0.00289	-560.0993	-270.9910	-8.0131	-3.8819	3.3256	-1.6101
	165.345	0.267821	0.00007	5365.5215	-581.9412	1.7742	-0.1927	-0.7363	-0.0799
	165.535	0.262000	0.00005	1519.3123	-802.2016	0.3511	-0.1856	-0.1457	-0.0770
K ₁	165.545	0.259851	-0.00730	1241.7937	-909.5249	-41.5484	30.4698	17.2433	12.6379
	165.555	0.257463	0.36878	1050.0000	-1050.0000	1758.4459	-1760.6741	-729.7842	-730.2731
	165.565	0.254755	0.05001	909.5249	-1241.7937	204.3862	-279.4065	-84.8237	-115.8892

	165.575	0.251757	-0.00108	802.2016	-1519.3123	-3.8472	7.2956	1.5967	3.0260
ψ_1	166.554	0.526244	0.00293	270.9910	560.0993	7.3700	15.2520	-3.0587	6.3261
	166.556	0.526104	-0.00004	270.9718	560.0173	-0.1056	-0.2185	0.0438	-0.0906
	166.564	0.466726	0.00005	260.6030	517.4666	0.1073	0.2133	-0.0445	0.0885
	167.355	0.335867	0.00018	172.1381	256.1130	0.1836	0.2735	-0.0762	0.1134
ϕ_1	167.555	0.328564	0.00525	155.5646	221.0708	4.7331	6.7347	-1.9643	2.7933
	167.565	0.327234	-0.00020	152.0845	214.1084	-0.1756	-0.2475	0.0729	-0.1026
	168.554	0.314689	0.00031	109.0991	137.7180	0.1877	0.2373	-0.0779	0.0984
θ_1	173.655	0.302004	0.00395	30.8765	32.8059	0.6497	0.6911	-0.2696	0.2867
J_1	175.455	0.301544	0.02062	26.8499	28.2971	2.9447	3.1073	-1.2221	1.2888
	175.465	0.301534	0.00409	26.7443	28.1798	0.5818	0.6138	-0.2414	0.2546
S_{01}	183.555	0.300244	0.00342	14.5605	14.9759	0.2637	0.2716	-0.1094	0.1126
O_{01}	185.555	0.300144	0.01129	13.4853	13.8409	0.8060	0.8283	-0.3345	0.3436
	185.565	0.300144	0.00723	13.4586	13.8127	0.5151	0.5294	-0.2138	0.2196

The periods of tesseral tides are coupled with the nodal period Ω of the satellite. Certain tidal components—most notably the K_1 tide—have period that coincide exactly with the nodal precession period, potentially interfering with the relativistic precession measurements. In calculating these periods, the direction of motion of the tidal component must also be considered (the sign before the period indicates its direction). The computed values are presented in Table 3. For example, the perturbation period of the K_1 tide on the orbits of both LARES 2 and LAGEOS coincides with the nodal precession periods of the two satellites (1050 days).

A comparison of the perturbation periods for both satellites in each row of Table 3 that when $m \neq 0$, the frequency coupling term $m(\dot{\Omega} - \dot{\theta})$ involving the satellite's nodal precession and Earth's rotation begins to contribute significantly to the inter-satellite asymmetry in tidal perturbation frequencies. Consequently, differences arise between the prograde and retrograde orbits. As a result, the effects of tesseral tides on Ω and i cannot be eliminated through a simple linear combination of two satellites. Instead, separate and precise tidal perturbation models must be developed for each satellite individually.

Table 4. Perturbation periods and amplitudes of the node and inclination for LAGEOS and LARES 2 satellites ($l=2, m=2, p=1, q=0$)

Tide name	Doodson number	Love number	$H_l^m(m)$	Perturbation periods		$\Delta\Omega_{lmpq}$ (mas)		Δi_{lmpq} (mas)	
				LAGEOS	LARES 2	LAGEOS	LARES 2	LAGEOS	LARES 2
	235.755	0.301083	0.01601	-6.9502	-6.7709	0.2452	-0.2391	0.6794	0.6627
	237.555	0.301083	0.01932	-7.1930	-7.0012	0.3063	-0.2983	0.8486	0.8269
	245.555	0.301083	-0.00389	-9.2680	-8.9519	-0.0795	0.0768	-0.2201	-0.2129
	245.645	0.301083	-0.00451	-9.2819	-8.9649	-0.0923	0.0892	-0.2556	-0.2472
N_2	245.655	0.301083	0.12099	-9.2946	-8.9768	2.4785	-2.3954	6.8667	6.6394
	247.455	0.301063	0.02298	-9.7340	-9.3860	0.4930	-0.4757	1.3658	1.3184
	255.545	0.301063	-0.02358	-13.9969	-13.2883	-0.7274	0.6910	-2.0152	-1.9153
M_2	255.555	0.301063	0.63192	-14.0257	-13.3143	19.5330	-18.5547	54.1159	51.4291
	263.655	0.301063	-0.00466	-25.0861	-22.8978	-0.2576	0.2353	-0.7138	-0.6522
	265.455	0.301063	-0.01786	-28.5667	-25.7630	-1.1244	1.0147	-3.1151	-2.8126
	265.555	0.301063	0.00359	-28.8215	-25.9701	0.2280	-0.2056	0.6318	0.5699

	265.655	0.301063	0.00447	-29.0809	-26.1805	0.2865	-0.2581	0.7937	0.7153
	265.665	0.301063	0.00197	-29.2058	-26.2817	0.1268	-0.1142	0.3513	0.3165
	271.557	0.301063	0.00070	-110.5386	-77.7839	0.1705	-0.1201	0.4724	0.3328
T ₂	272.556	0.301063	0.01720	-158.5079	-98.8303	6.0084	-3.7488	16.6462	10.3907
S ₂	273.555	0.301063	0.29400	-280.0292	-135.4907	181.4391	-87.8472	502.6752	243.4916
R ₂	274.554	0.301063	-0.00246	-1200.0795	-215.3872	-6.5062	1.1685	-18.0253	-3.2388
	274.556	0.301063	0.00062	-1200.4562	-215.3993	1.6403	-0.2945	4.5444	0.8163
	274.566	0.301063	-0.00004	-1457.8909	-222.4473	-0.1285	0.0196	-0.3561	-0.0544
	275.455	0.301063	0.00019	626.8389	-451.6268	-0.2625	-0.1892	-0.7272	0.5245
	275.545	0.301063	0.00103	568.9358	-487.3636	-1.2915	-1.1070	-3.5780	3.0684
K ₂	275.555	0.301063	0.07996	525.0000	-525.0000	-92.5151	-92.5770	-256.3120	256.6015
	275.565	0.301063	0.02383	487.3636	-568.9358	-25.5951	-29.8991	-70.9111	82.8733
	277.555	0.301063	0.00063	135.4907	280.0292	-0.1881	0.3891	-0.5212	-1.0784
	275.575	0.301063	0.00259	454.7624	-620.8969	-2.5958	-3.5464	-7.1915	9.8298
	285.455	0.301063	0.00447	26.1805	29.0809	-0.2579	0.2867	-0.7145	-0.7946
	285.465	0.301063	0.00195	26.0800	28.9570	-0.1121	0.1245	-0.3105	-0.3452

For sectorial earth tides, the computed results are presented in Table 4. Among all sectorial tides, the K₂ and S₂ components are the most critical: they exhibit both the largest perturbation amplitudes and the longest periods. This means that any inaccuracies in the modeling these two tides (i.e., an inability to precisely represent their effects on satellite orbits) can significantly compromise the high-precision measurement of relativistic effects on the satellites' orbits.

In addition, for the perturbations of the 3rd-degree Earth tides, we calculated the 10 significant tidal constituents with astronomical amplitudes of no less than 0.001 m listed in Tables 5(a) to 5(d) of Cartwright and Tayler (1971), whose Doodson numbers are 065.555, 135.555, 155.555, 175.555, 235.655, 245.555, 265.555, 345.655, 355.555 and 375.555, respectively. The mode with $(l, p, q) = \{(3, 0, 0), (3, 1, 0), (3, 2, 0), (3, 3, 0)\}$ were adopted for the calculations. For the perturbations of the ascending node, only the two modes to LARES 2 reach the magnitude of tenths of a milliarcsecond: 265.555 for $(l, m, p, q) = (3, 2, 1, 0)$ and 065.555 for the $(l, m, p, q) = (3, 2, 2, 0)$, with the values being -0.3285 mas (-69.9868 days) and 0.3831 mas (80.7517 days), respectively. For the perturbations of the orbital inclination, none of the above tidal constituents attains the preset threshold. The perturbation amplitudes of the remaining 3rd-order Earth tide modes are extremely small, falling in the range of 10^{-10} to 10^{-5} mas, which are far below the screening threshold; therefore, no further elaboration on these modes is presented in this paper.

The screening method using the threshold calculated from the RMS of overlap orbit differences, which objectively measures the contribution of individual tidal constituents, has inherent shortcomings — the cumulative contribution of the filtered secondary tidal constituents to the target orbital elements exceeds the aforementioned threshold, as shown in Figs. 4 and 5. This reflects the general drawbacks of such individual tidal constituent screening approaches: the coherent temporal superposition of massive tiny constituents (In particular, secondary tidal perturbations with perturbation periods of half a month and about a month), frequency cluster-orbital resonance coupling, and collective detectability may lead to the total superimposed effect exceeding the threshold, a phenomenon particularly significant for high-precision satellites like LAGEOS/LARES 2. Therefore, it is necessary to reconsider incorporating these secondary tidal constituents into the tidal perturbation modeling framework and evolve the selection principle from “isolated constituent judgment” to “collective superimposed effect evaluation”. Specifically, based on the internal consistency accuracy of orbit determination (RMS of overlap orbit differences), the threshold should be redefined as the “minimum negligible limit of total collective effect”, extending to dual-dimensional screening (time domain + frequency domain). In practice, a closed-loop strategy should be adopted: hierarchical coarse screening by Doodson-coded frequency clusters, verification of total superimposed effect, a dual-threshold system (single-constituent amplitude + total superimposed effect), and orbit determination back-substitution validation. The core criterion is that only when the total superimposed effect of constituent clusters is lower than the orbit determination accuracy threshold can the relevant constituents be safely

excluded, which is consistent with the IERS 2010 Conventions and the requirements of high-precision satellite orbit determination.

Naturally, minimizing the difference between the satellite ascending node time series (after deducting various classical perturbations) and the theoretical frame dragging effect is only the original intention of this work. When evaluating the final results, there are two types of assessment methods: one based on fitting residuals (a more direct method starting from numerical results) and the other based on the uncertainty of physical models (a more rigorous method that requires propagating the uncertainty of each tidal constituent to the final orbital residuals via the law of error propagation). Thus, from the perspective of the error propagation assessment method, it is not better to deduct more tidal constituents, but to achieve a balance that considers both numerical performance and uncertainty—i.e., maximizing numerical gain while minimizing uncertainty propagation. However, strictly evaluating the uncertainty of each tidal constituent is extremely challenging; a feasible compromise is to use statistical resampling methods such as Monte Carlo simulation for estimation.

In addition to the screening approach, the impact of tidal perturbations on the accuracy of the Lense-Thirring effect detection arises from two sources: (1) limitations in the tidal perturbation model itself (for example, discrepancies between Kaula’s linear perturbation theory and the actual tidal perturbations), and (2) uncertainties inherent in the tides (such as errors in Love numbers or in ocean tide models). The assessment of how to correct for tidal perturbations affects the detection accuracy of the Lense-Thirring effect is an important direction for future work and lies beyond the scope of this paper.

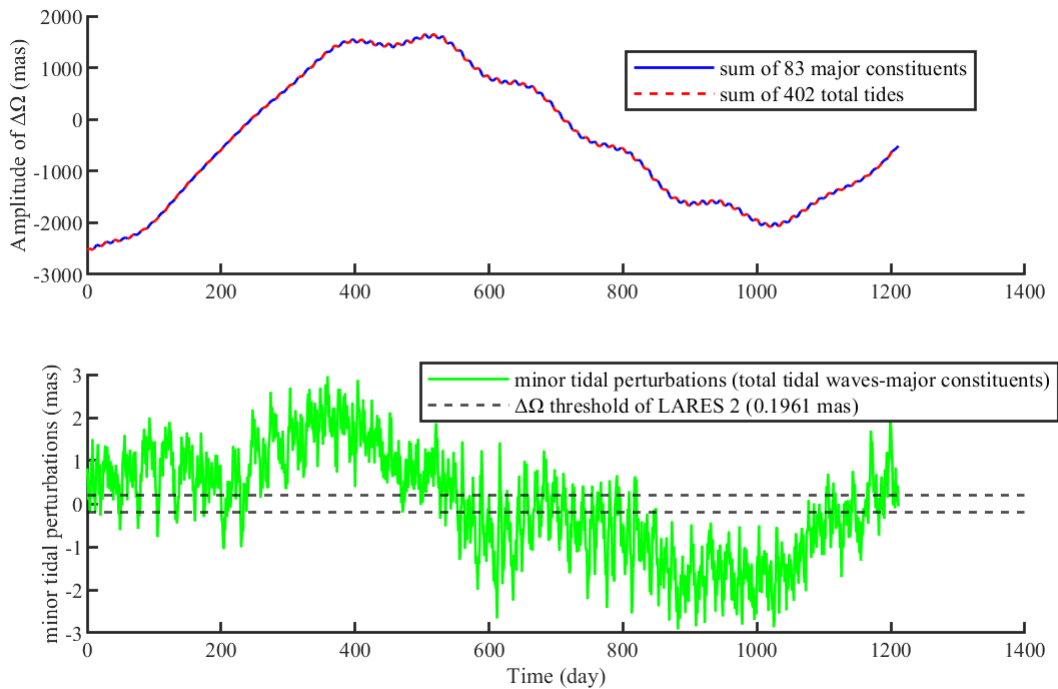


Fig. 4 Comparison of tidal perturbations on Ω of LARES 2: sum of 83 major constituents vs. sum of 402 total tides

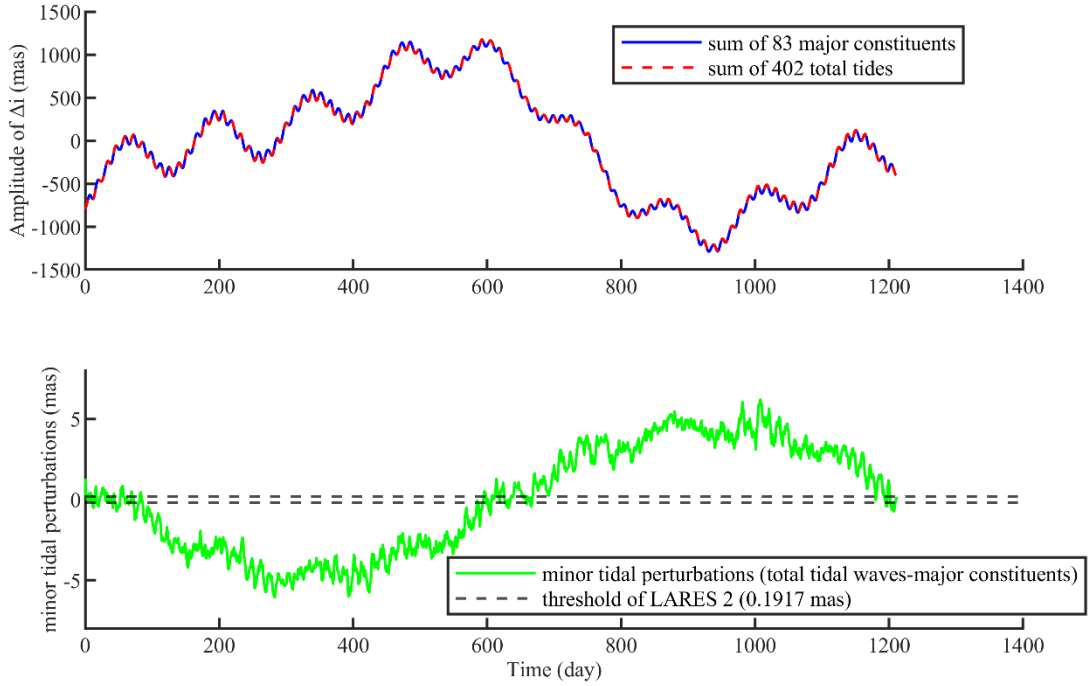


Fig. 5 Comparison of tidal perturbations on i of LARES 2: sum of 83 major constituents vs. sum of 402 total tides

Conclusions and Outlook

This study, based on Kaula perturbation theory and Lagrange's equations, systematically derived the formulas for Earth tidal perturbations on the right ascension of the ascending node (Ω) and orbital inclination (i) of LARES 2 and LAGEOS satellites. By selecting 83 earth tides with significant tidal perturbation modes from 402 earth tide constituents, it quantitatively analyzed the asymmetric tidal perturbation characteristics between the two satellites, providing critical support for high-precision General Relativity verification and satellite orbital dynamics research.

Essentially, tidal perturbation asymmetry arises from differing relative angular velocities between satellite nodal precession and Earth's rotation for prograde/retrograde orbits; consequently, the same tide exhibits period and amplitude asymmetry on two satellites due to these frequency differences, disrupting the classical perturbation cancellation effect of the "butterfly configuration" and requiring individual modeling of $m \geq 1$ tesseral/sectorial tides (e.g., K_1 and S_2) for each satellite.

Further, differential response characteristics by tidal type: Zonal tides exhibit consistent periods and "equal in magnitude but opposite in sign" $\Delta\Omega$ responses, allowing partial cancellation through combination. Tesseral and Sectorial tides show period and amplitude difference. Hierarchy of perturbation source contributions: Earth tides are dominated by $l=2$ order components, with K_1 , S_2 as the primary interference sources. However, the cumulative contribution of the filtered secondary tidal constituents to the target orbital elements should not be ignored.

Building on these conclusions, future research will focus on three directions. First, this study is based on linear tidal theory, neglecting nonlinear interactions of tides. Future work should derive nonlinear tidal perturbation potentials through fluid dynamics equations, introducing nonlinear tidal coefficients to quantify nonlinear effects on satellite orbits. Second, the conventional single-amplitude threshold for Earth tide constituent selection is limited, tiny constituents' coherent superposition and frequency-orbital resonance push total effect over the threshold, so we propose shifting to collective effect evaluation via a time-frequency dual-dimensional closed-loop strategy, excluding only clusters with total effect below orbit determination accuracy. Additionally, Long-term observational validation: LARES 2 has accumulated approximately 3 years of laser ranging data since its

launch in July 2022. Future work should combine this with LAGEOS's 30-year long-term data to invert actual tidal perturbation amplitudes and periods through orbital fitting, validating theoretical model accuracy and correcting Love numbers k_2 .

Acknowledgements

This study is supported by National Science and Technology Major Project for Deep Earth Research (Grant 2024ZD1002700), the Central-to-Local Science and Technology Development Special Project in Hubei Province (Grants 2025CFC006), the National Precise Gravity Measurement Facility (Huazhong University of Science and Technology) (Grant PGMF-2024-Z003), Theory of Hydrocarbon Enrichment under Multi-Spheric Interactions of the Earth (Grants THEMSIE). We are also grateful for the support from the Scuola di Ingegneria Aerspaziale of Sapienza University of Rome (Italy), Lanzhou University and International Center for Theoretical Physics Asia-Pacific.

Author contributions

The authors declare no conflict of interest. Xizhi Hu, under the guidance of Ignazio Ciufolini and Xiaodong Chen, defined the scientific objectives of this study and designed the specific research plan. Xiaodong Chen, Ignazio Ciufolini, Wei-Tou Ni, and Jianqiao Xu participated in the adaptation and optimization of the research methodology, as well as in-depth discussions of the results. Xizhi Hu implemented the programming and numerical computations based on established methods, supplemented new analytical results, integrated data from previous studies, and drafted the initial manuscript. Wei-Tou Ni, Antonio Paolozzi, Jianqiao Xu, and Xiaodong Chen critically reviewed and revised the manuscript for important intellectual content. All authors reviewed the manuscript and contributed individually to the writing.

Funding

This work was funded by National Science and Technology Major Project for Deep Earth Research (Grant 2024ZD1002700); the Central-to-Local Science and Technology Development Special Project in Hubei Province (Grant 2025CFC006); the National Precise Gravity Measurement Facility (Huazhong University of Science and Technology) (Grant PGMF-2024-Z003); Theory of Hydrocarbon Enrichment under Multi-Spheric Interactions of the Earth (Grant THEMSIE).

Data availability

The orbital element data of LARES 2 and LAGEOS used in this study are derived from satellite laser ranging (SLR) observations processed by the GEODYN II and UTOPIA orbit estimators (Ciufolini et al., 2023). The Earth tide constituent data are based on the Cartwright and Tayler (1971) convention. All numerical calculation results and key tidal perturbation parameters supporting the findings of this study are included in the published article and its supplementary tables. The raw SLR observation data are available from the corresponding author on reasonable request.

References

- Bertotti B, Carpino M (1989) Measurement of the gravitomagnetic field using a pair of laser ranged satellites. In: ASI final report. ASI, Frascati, p 105
- Cartwright DE, Tayler RJ (1971) New computations of the tide-generating potential. *Geophys J R Astron Soc* 23:45–73. <https://doi.org/10.1111/j.1365-246X.1971.tb01803.x>
- Cartwright DE, Edden AC (1973) Corrected tables of tidal harmonics. *Geophys J Int* 33:253–264. <https://doi.org/10.1111/j.1365-246X.1973.tb03420.x>
- Ciufolini I (1986) Measurement of the Lense-Thirring drag on high-altitude, laser-ranged artificial satellites. *Phys Rev Lett* 56(4):278–281. <https://doi.org/10.1103/PhysRevLett.56.278>
- Ciufolini I, Wheeler JA (1996) *Gravitation and Inertia*. Princeton University Press, Princeton

- Ciufolini I, Chiappa F, Lucchesi D, Vespe F (1997) Test of Lense-Thirring orbital shift due to spin. *Class Quantum Grav* 14:2701–2726. <https://doi.org/10.1088/0264-9381/14/10/003>
- Ciufolini I, Pavlis E (2004) A confirmation of the general relativistic prediction of the Lense–Thirring effect. *Nature* 431:958–960. <https://doi.org/10.1038/nature03007>
- Ciufolini I, Paolozzi A, Pavlis EC, et al (2017) A new laser-ranged satellite for General Relativity and space geodesy: I. An introduction to the LARES experiment. *Eur Phys J Plus* 132(336):1–9. <https://doi.org/10.1140/epjp/i2017-11635-1>
- Ciufolini I, Paolozzi A, Pavlis EC, et al (2023) The LARES 2 satellite, general relativity and fundamental physics. *Eur Phys J C* 83(87):1–10. <https://doi.org/10.1140/epjc/s10052-023-11230-6>
- Ciufolini I, Paris C, Pavlis EC, et al (2024) On the high accuracy to test dragging of inertial frames with the LARES 2 space experiment. *Eur Phys J C* 84(10):1–15. <https://doi.org/10.1140/epjc/s10052-024-13301-8>
- Doodson AT (1921) The harmonic development of the tide-generating potential. *Proc R Soc A* 100:305–329. <https://doi.org/10.1098/rspa.1921.0088>
- Dziewonski AM, Anderson DL (1981) Preliminary reference Earth model. *Phys Earth Planet Interiors* 25(4):297–356. [https://doi.org/10.1016/0031-9201\(81\)90046-7](https://doi.org/10.1016/0031-9201(81)90046-7)
- Eanes RJ (1983) Earth and ocean tide effects on Lageos and Starlette. In: *International Symposium on Earth Tides* eds. E Sckweizerbart'sche Verlagabuchhandlung, Stuttgart, pp 239–249
- Efroimsky M, Williams JG (2009) Tidal torques: a critical review of some techniques. *Celest Mech Dyn Astron* 104(3):257–289. <https://doi.org/10.1007/s10569-009-9204-7>
- Gurzadyan VG, Ciufolini I, Khachatryan HG, et al (2017) On the Earth's tidal perturbations for the LARES satellite. *Eur Phys J Plus* 132:548. <https://doi.org/10.1140/epjp/i2017-11839-3>
- Gurzadyan VG, Ciufolini I, Khachatryan HG, et al (2025) On the Earth's tidal perturbations. II. LARES 2 satellite. *Eur Phys J Plus* 140:512. <https://doi.org/10.1140/epjp/s13360-025-06458-y>
- Kaula WM (1961) Analysis of gravitational and geometric aspects of geodetic utilisation of satellites. *Geophys J* 5:104–133. <https://doi.org/10.1111/j.1365-246X.1961.tb00417.x>
- Kaula WM (1964) Tidal dissipation by solid friction and the resulting orbital evolution. *Rev Geophys* 2:661–684. <https://doi.org/10.1029/RG002i004p00661>
- Kaula WM (1966) *Theory of Satellite Geodesy*. Blaisdell Publ Co, Waltham
- Lense J, Thirring H (1918) Über den einfluss der eigenrotation der zentralkörper auf die bewegung der planeten und monde nach der einsteinschen gravitationstheorie. *Phys Z* 19:156–163. <https://www.physics.rutgers.edu/~sergei/617/LT.pdf>
- Love AEH (1926) *A Treatise on the Mathematical Theory of Elasticity*. Dover Publ, New York
- Lyard F, Lefevre F, Letellier T, et al (2006) Modelling the global ocean tides: modern insights from FES2004. *Ocean Dyn* 56:394–415. <https://link.springer.com/article/10.1007/s10236-006-0086-x>
- Mathews PM, Herring TA, Buffett BA (2002) Modeling of nutation and precession: New nutation series for nonrigid Earth and insights into the Earth's interior. *J Geophys Res* 107(B4):ETG3-1–ETG3-26. <https://doi.org/10.1029/2001JB000390>
- Melchior P (1983) *The tides of the planet Earth*, 2nd edn. Pergamon Press, London
- Petit G, Luzum B (2010) IERS conventions. Technical Report. IERS Technical Note No. 36, Paris
- Sanchez BV (1975) *Rotational dynamics of mathematical models of the nonrigid earth*. Dissertation, Texas Univ, Austin
- Shao K, An Z, Yang Y, Yi B (2025) Precise multi-satellite orbit and geodetic parameter determination using satellite laser ranging observations from LAGEOS, Etalon and newly launched LARES-2. *Meas Sci Technol* 36(2):026319. <https://iopscience.iop.org/article/10.1088/1361-6501/adac00>
- Wahr J (1981) Body tides on an elliptical, rotating, elastic and oceanless earth. *Geophys J Int* 64:677–703. <https://doi.org/10.1111/j.1365-246X.1981.tb02690.x>
- Wahr J, Sasao T (1981) A diurnal resonance in the ocean tide and in the Earth's load response due to the

- resonant free 'core nutation'. *Geophys J Int* 64(3):747–765. <https://doi.org/10.1111/j.1365-246X.1981.tb02693.x>
- Wahr J, Bergen Z (1986) The effects of mantle anelasticity on nutations, earth tides, and tidal variations in rotation rate. *Geophys J Int* 87(2):633–668. <https://doi.org/10.1111/j.1365-246X.1986.tb06642.x>
- Widmer R, Masters G, Gilbert F (1991) Spherically symmetric attenuation within the Earth from normal mode data. *Geophys J Int* 104(3):541–553. <https://doi.org/10.1111/j.1365-246X.1991.tb05700.x>